PFC/JA-89-18

Plasma Flow Measurements Along the Presheath of a Magnetized Plasma

Chung, K.S., Hutchinson, I.H., LaBombard, B. and Conn, R.W.

Plasma Fusion Center
Massachusetts Institute of Technology
Cambridge, MA 02139

March 1989

Submitted to: Physics of Fluids

This work was supported by the U. S. Department of Energy Contract No. DE-AC02-78ET51013. Reproduction, translation, publication, use and disposal, in whole or in part by or for the United States government is permitted.

PLASMA FLOW MEASUREMENTS ALONG THE PRESHEATH OF A MAGNETIZED PLASMA.

by

K-S.Chung and I.H.Hutchinson

Plasma Fusion Center,

Massachusetts Institute of Technology, Cambridge, Massachusetts, U.S.A.

B.LaBombard* and R.W.Conn

Institute of Plasma Fusion Research,

University of California, Los Angeles, California, U.S.A.

Plasma flow measurements in the presheath have been performed using two types of directional electric "Mach" probes, in the PISCES facility at UCLA. A fast scanning versatile probe combination has been developed, which operates simultaneously as a "magnetized" Mach probe, an "unmagnetized" Mach probe(with characteristic probe size greater than and smaller than ion gyroradius, respectively), and an emissive probe. Presheaths have been investigated by inserting a small object at the center of the plasma column. Variations in plasma flow velocity, density, and potential along the presheath have been deduced by fluid and kinetic theories. A comparison is made between Mach numbers obtained from the magnetized probe and the unmagnetized probe. Incorporation of shear viscosity of order $\sim 0.5nm_iD_\perp$ in the cross-field transport along the presheath seems best to model the results. The cross-field diffusivity($D_\perp$) is found to scale approximately proportional to $B^{-1/2}$, with magnitude about 4 times larger than Bohm, in the PISCES plasma. The effect of an electrical bias applied to the object on the presheath characteristics is discussed.

*Present address : Plasma Fusion Center, M.I.T., Cambridge, MA, U.S.A.

I. INTRODUCTION

It has become clear that the edge conditions are important in influencing the characteristics of magnetically confined fusion research plasmas. Interaction of the edge plasma with the material edge structures determines the purity and hence stability of the plasmas[1,2]. The edge conditions can also influence the global parameters such as energy confinement time and beta poloidal directly, for example, in determining the difference between the L- and the H-modes[3]. A feedback mechanism by which confined plasma tends to self-regulate its edge conditions has been investigated[4,5], and recently the inter-relationship between the edge and the global parameters has been studied for the JET[6,7]. Significant ion drift due to scrape-off flow may play an important role in impurity transport and fluctuation levels and in the design of divertor and limiters in fusion devices[8,9]. Many measurements have also shown large asymmetries in the ion saturation current drawn to probe faces parallel and antiparallel to the magnetic field[10,11]. These appear to be caused primarily by the presence of plasma flow along the field. This plasma flow makes the interpretation of the probe measurements difficult because of the absence of a fully verified probe theory. It is the purpose of the present work to explore the physics of both the edge plasma processes themselves and the measurement of the plasma by probes.

Harbour and Proudfoot measured the plasma flow velocity by using a two sided directional probe("Mach" probe) in the DITE tokamak[8]. They used an empirical formula to interpret their data, since the fluid model without viscosity[12,13] seemed to overestimate the flow velocity for their measurements. Matthews *et al.* investigated the presheath in the wake of large object in the DITE tokamak in order to deduce the cross-field diffusivity[14]. They observed data consistent with cross-field diffusivity similar to the Bohm diffusivity with assumption of equal radial and poloidal cross-field diffusion coefficients. LaBombard *et al.* measured the flow velocity and the density along the presheath in the PISCES

facility[15]. Their data suggested that shear viscosity effects did not strongly dominate in the presheath plasma flow and the data was perhaps fit better by a fluid model without viscosity than with viscosity.

The presheaths produced in the last two experiments are not "free" (i.e., extending a distance along the magnetic field determined by cross-field transport), but bounded by the structures such as the limiter or cathode. In other words, the perturbing object is large enough that its free perturbation length would be longer than the geometric distance between the object and the other structure(limiter or cathode). The objective of this work is to generate a free presheath due to the perturbing object. Then the same theory can be applied consistently to the free presheath of the perturbing object and to the presheath of the magnetized probe used to diagnose the object's presheath. Thus the self-consistency of theory and experiment can be explored.

We have performed plasma flow measurements in the free presheath using two types of directional electric Mach probes, in the PISCES facility at UCLA[16]. Presheaths have been investigated by inserting a small object at the center of the plasma column. A fast scanning versatile probe combination has been developed, which operates simultaneously as a "magnetized" Mach probe with probe radius(a) greater than the ion gyroradius(ρ_i), an "unmagnetized" Mach probe($a < \rho_i$), and an emissive probe. Ion current densities at the upstream and downstream sides, space potential, and floating potential are measured in two dimensions. Variations in plasma flow velocity, density, and potential along the presheath have been deduced from these measurements. The effect on the presheath characteristics either of an electrical bias applied to the object or of an external magnetic field has been investigated.

A variety of competing one dimensional fluid theories[12,13,17–19] for magnetized Mach probes exists; the main source of the substantial differences between these is the assumption about shear viscosity[18]. We have also developed kinetic theories[20,21] for the magnetized

Mach probe. In this paper, predictions from the kinetic theory are compared with experimental results. Data from the magnetized probe are analyzed self-consistently, based upon a generalized kinetic model. A comparison is also made between Mach numbers deduced from the magnetized probe and the unmagnetized probe measurements. Unfortunately, the theory of unmagnetized probes for flow measurement is by no means well established, but the comparison with what interpretation theory exists provides a valuable additional calibration.

In section II, the experimental set up and diagnostics are outlined. Section III deals with the experimental data and their analyses. Part A of section III introduces the models which we have applied to the interpretation of the measurement. In part B, we interpret the measured data based upon prevailing theories. Part C shows the determination of characteristic parameters such as cross-field diffusivity and ion collection length. Part D deals with the effect on the current density ratio due to variations of magnetic field intensity and electrical bias of the perturbing object. Section IV summarizes the results.

II. EXPERIMENTAL SETUP and DIAGNOSTICS

Plasma is produced by a reflex discharge between a hot LaB_6 cathode and a water-cooled annular copper anode at one end of the chamber[22]. Steady-state plasmas with densities 10^{11} to 10^{13} cm^{-3} and electron temperatures of 3 to 30 eV are readily achieved in a 6 to 10 cm diameter cylindrical column of approximately 100 cm long. For the data presented here, helium discharges of $T_e = 6 - 10eV$, $T_i \approx 0.8eV$, $n_e = 2 - 4 \times 10^{12} cm^{-3}$, and $B = 400 - 1400G$ were used. A free presheath is formed by inserting a small perturbing object at the center of this cylindrical column. Fig. 1 shows the schematic setup for ion flow measurement. The alignment of the perturbing object and the fast scanning probe is made through two viewing ports.

Plasma diagnostics and generation of the presheath are shown in Fig. 2. A stationary, water-cooled Langmuir probe was inserted into the plasma stream and was typically used to deduce the electron density and temperature from a complete current-voltage characteristic at a fixed position. An Optical Multichannel Analyzer(OMA) was used to measure the ion temperature during these experiments using Doppler broadening. A He^{II} line at 4686 $\AA$ was observed in second order to provide sufficient resolution for the rather low ion temperature($\approx 0.8\ eV$).

A pneumatic cylinder was used to drive a versatile probe tip across the plasma column, typically 10 cm in diameter, and back(15 cm stroke) within 400 msec(see Fig. 3). This enabled a vertical profile to be taken in one stroke and at the same time limited the total energy deposited on the probe to safe levels during the high density plasmas that can be achieved in PISCES(power fluxes $> 400 W/cm^2$). A differentially-pumped sliding seal allowed the probe to be positioned for a fast vertical scan at various axial distances from the object surface. By vertically scanning the plasma column through its centerline at uniformly spaced axial locations, a complete map of plasma parameters in the near presheath of the object was assembled. The system could access any point in a 10x10x10 cm volume.

A unique probe tip that functions simultaneously as two types of Mach probe and as an emissive probe was constructed for these experiments. The probe tip simply consisted of a 6.3 mm diameter 6-hole extruded alumina rod with a specially sculptured end(see Fig.4). The Mach probe is a directional probe which measures separately the currents collected parallel and antiparallel to the magnetic field. Two 1 mm diameter molybdenum wires of 3.7 mm of exposed length were used to collect particles on opposing sides of an alumina separator. Since the whole probe tip(6.3 mm diameter) perturbs the plasma, two separated molybdenum wires behaved like a "magnetized" Mach probe(typical ion gyroradius of helium plasma in PISCES is $\sim$ 1.3 mm for B = 1400 G). Two tungsten

plasma column, i.e., around $x = 0cm$, $z = 0cm$. The magnetic field is parallel to the z coordinate.

Floating potential of the emissive probe is shown in Fig. 6, for the case of strong electron emission(hot filament) and no electron emission (cold filament). For the purposes of analysis here, the floating potential of the emissive probe during strong electron emission is designated as the "plasma space potential". Tests show that the actual plasma potential may differ from this value by an amount equal to $\simeq 1.5T_e$, due to a double sheath which forms in front of the probe[23,24]. However, since we are concerned in this work with the variation of the plasma potential along the z-direction where $T_e \simeq$ constant, we need not consider this correction to the raw data.

Fig. 7 shows data obtained along the presheath at the center of the perturbing object. The upstream and downstream sheath current densities are measured by the magnetized and the unmagnetized probes. The ratios of sheath current densities, space potential, and floating potential are also shown.

A) Presheath Models

One dimensional theoretical presheath models consist of some kind of self-consistent solution to either the continuity and momentum equations(fluid models) or the Boltzmann equation(kinetic models) together with Poisson's equation. The cross-field transport is modelled via sources in the presheath. The main differences between theories are attributable to different assumptions about these sources[18].

For the magnetized probe, we have extended our previous kinetic theory[20] by introducing a generalized source term as

$$S_f = W(z,v)[\alpha\{f_\infty(v) - f(z,v)\} + (1-\alpha)(1 - \frac{n(z)}{n_\infty})f_\infty], \qquad (1)$$

where α is the equivalent ratio of viscosity to diffusivity[18].

The idea here is that there is a certain amount of particle exchange, represented by the first term that we have been working with up to now, plus a certain amount of particle inflow, represented by the second term. The inflow is presumably caused by the fact that the density is different inside the collection tube, so it is proportional to the density difference. The distribution of the inflowing particles is that of the external plasma. Obviously, $\alpha = 0$ corresponds to pure inflow (no viscosity) and $\alpha = 1$ to pure exchange. The rate of particle and momentum exchange between the outside and the inside of the flux tube is taken to be equal, representing random migration of ions in either direction. The rate is related via

$$W \sim \frac{D_\perp}{a^2}, \tag{2}$$

to $D_\perp$ the anomalous cross-field diffusion coefficient and a the radius of the probe. We have also used two fluid models, one is equivalent to no viscosity ($\alpha = 0$) case and the other is the $\alpha = 1$ case. The results are quite similar to the corresponding kinetic models.

For the unmagnetized probe, we adopt the Hudis and Lidsky's fluid model[25] which is based upon the free fall model of ions for collisionless streaming plasma with low ion temperature($T_i < T_e$).

Sheath currents are measured at each side of the probe in Mach probes. The ratio of the measured upstream(j_{sup}) and downstream(j_{sdown}), ion sheath current densities is obtained as

$$R = j_{sup}/j_{sdown}. \tag{3}$$

We have found [20] that the Mach probe calibration for the upstream to downstream current ratio, R, as a function of normalized velocity $V = v/(T_e/m_i)^{1/2}$ can be written for the various theories quite accurately as

$$R = exp[KV], \tag{4}$$

where the constant K depends on the assumptions of the model(e.g. α). Hence the unperturbed flow velocity along the presheath, generated by the perturbing object, can be obtained as

$$V = \frac{1}{K} ln[R], \tag{5}$$

where the values of K for the various kinetic models are as follows: For $T_i = 0.1T_e$, $K = 1.26, 1.81$, and 2.07 for $\alpha = 0.0, 0.5$, and 1.0, respectively. From the fluid models K is obtained as 1.0 and 2.27 for equivalent $\alpha = 0.0$ and 1.0, respectively. For the unmagnetized Mach probe, K is given by ≈ 1.26 for $T_i = 0.1T_e$ from the Hudis and Lidsky model[25].

If we deduce the flow velocity V according to the various models, we can calculate the unperturbed ion density as

$$N = (j_{sup} + j_{sdown})/2f(V), \tag{6}$$

where $f(V)$ is a ratio of the mean ion current density to the unperturbed ion density at z, which is dependent on the model, but only rather weakly. Usually $f \simeq 0.5(T_e/m_i)^{1/2}$.

B) Interpretation of Data

To compare our values with the flow velocity and density along the presheath, we would like to have independent measurements of the relevant parameters from diagnostics such as laser-induced fluorescence. Unfortunately, we do not have this data so instead we interpret the probe data using the different models and compare them with each other. Two types of presheath are formed; one is due to the perturbing object and the other is due to the probe(see Fig.8). The raw data of Figs. 5-7 will be analyzed.

Since we are interested in the variation of plasma parameters along the presheath(i.e., along the magnetic field line), we will concentrate on the measurements along the axis of the perturbing object. The upstream- and downstream-side probe areas are calibrated relative to each other(see Appendix).

Fig. 9 shows the flow velocity deduced from the measurement by the magnetized Mach probe along the presheath according to different models, expressed as a Mach number; i.e. normalized by $c_s = [(T_e + T_{i\infty})/m_i]^{1/2}$. Since the Mach number at the sheath is not expected to exceed one, the Mach numbers derived from the Stangeby(zero viscosity) and free-fall (zero ion temperature and zero source) models seem too large, while others are very similar. We also include the Mach number deduced from the measurement by the unmagnetized Mach probe along the same presheath, which is independent of the measurement by the magnetized Mach probe. It seems to agree with those deduced by the viscid models. Thus the data of Fig. 9 suggests that shear viscosity plays an important role in the presheath of the magnetized plasma. A viscosity of order $\nu \sim 0.5nm_iD_\perp$ seems to give the most plausible interpretation of the data.

In Fig. 10, the density along the presheath is shown. The deduced density variation along the presheath is almost independent of the interpretation model. The density measured by the unmagnetized Mach probe also agrees very well with the magnetized probe data, confirming the mutual consistency of the models for density measurement.

From these analyses, we have observed that the flow velocity interpretation strongly depends on model, while the density interpretation depends weakly on model.

C) Characteristic Parameters – Self-Consistent Analysis

We have developed a self-consistent analysis for the magnetized probe based upon a generalized kinetic model because we have not been convinced that the model for the unmagnetized probe is reliable as an independent measurement. Since there are two free presheaths formed: due to the object, and due to the probe, we look for a model which succeeds in explaining both presheaths simultaneously. Fig. 11(A) shows the measured sheath current density ratios along the presheath region of the perturbing object. Fig. 11(B) shows the densities measured by the unmagnetized Mach probe. Here we have

estimated the densities by simply averaging the ion saturation currents collected on the upstream and downstream facing probes. This is the same treatment as the previous analysis[15] and can be justified by the weak dependence of density upon the various models which was shown in part (B). The different symbols represent data obtained under different conditions: different perturbing objects and intensity of the magnetic field (from 1000 gauss to 1400 gauss); electron temperature between 7 and 10 eV; ion temperature of $\approx 0.8eV$; He gas pressure of $\approx 10^{-3}$ torr; and plasma density ranging from 2 to $4\times10^{12}cm^{-3}$. These data can be reasonably compressed into a 'universal' curve, as the plots show, by normalizing the parallel distance relative to the presheath connection length $L_{cd} \equiv a_d^2(T_e/m_i)^{1/2}/D_\perp$ with $D_\perp$ taken as the Bohm value($D_{Bohm} = kT_e/16eB$), where a_d is the radius of the object. However, the total variation of L_{cd} over the different conditions is only 23%, so that exact scaling is not established by these data.

Our kinetic theory, applied to the object's presheath, predicts a certain variation of drift velocity and density with distance. Taking $W = D_\perp/a^2$ and adopting the Bohm diffusion value sets the parallel length scale. Simultaneously applying the theory to the probe's presheath provides us with the calibration factor K(of Eq. 4) and hence we obtain a theoretical value of R as well as N, versus z/L_{cd}. The theoretical lines for $D_\perp = D_{Bohm}$ are shown in Fig. 11(upper scale). The fit is poor. However, it is reasonable to regard the diffusion coefficient, $D_\perp$, as a free parameter in this fitting process. By altering its assumed value(still scaling $\propto D_{Bohm}$), we alter L_{cd} and hence scale the longitudinal coordinate. The theoretical lines for $D_\perp = 4D_{Bohm}$ are also shown in Fig. 11(bottom scale). This choice provides approximately the best theoretical fit to the data. Of the two curves, the $\alpha = 1$ curve seems to fit somewhat better than $\alpha = 0$, especially closer to the object, although the fit is clearly not fully satisfactory.

In Fig. 12(A), space potential variation(normalized by $\eta \equiv -e\phi/T_e$) is shown together with the theoretical prediction for $D_\perp = 4D_{Bohm}$. Fig. 12(B) shows the space potential

deduced from the measured densities of Fig. 11(B) assuming a Boltzmann relation. It seems to fit with the model quite well. The variation of the space potential along the presheath measured by the emissive probe seems to be inconsistent with that of the deduced potential from densities, indicating either a deviation from Boltzmann electrons or some problem with the potential interpretation. Choosing the cross-field diffusion coefficient to be 4 times larger than Bohm based on our fitting, we obtain the characteristic parameters as the following: $D_\perp = 1.4 - 1.9 \times 10^5 cm^2 sec^{-1}$, $L_{cd} = 3.5 - 6.3 cm$, and $L_{cp} = 0.7 - 0.9 cm$, where L_{cd} and L_{cp} are the ion collection length due to the perturbing object and the probe, respectively. If the probe is very close to the object($z \leq L_{cp}$), the presheath due to the probe is no longer free, rather it is bounded, since the perturbation due to the probe is intercepted by the object. Since all models apply only for a Mach probe with unbounded presheaths, one should be cautious when comparing the data at $z \leq L_{cp}$ with theory.

D) Magnetic Field and Electrical Bias Effects

We have explored the variation of the presheath of a fixed object with magnetic field over a much wider range: $400G \leq B \leq 1400G$. Fig. 13 shows the variation in the object's presheath current ratio with the magnetic field. We focus only on the unmagnetized probe data because it always remained in the unmagnetized($a < \rho_i$) regime, while the magnetized probe became unmagnetized at low B. Fig. 13(A) shows the variation versus unnormalized longitudinal position. If we normalize distance by L_{cd} based upon the assumption $D_\perp = 4D_{Bohm}$, we get Fig. 13(B). This does not fully compress the data onto a single curve, indicating that diffusion is not scaling proportional to D_{Bohm}(i.e., $\propto T_e/B$). If, instead, we take a collection length based on $D_\perp \propto D_{Bohm}^p$, with p an adjustable parameter, we get a reasonable universal fit for $p = 0.5$, as shown in Fig. 13(C). Since this is simply a scaling procedure, we cannot obtain the absolute coefficient of cross-field diffusivity. This scaling(i.e. $p = 0.5$) does not substantially affect our previous results in Fig. 11, because

of the very small range in B, and hence L_{cd}, for which they were obtained.

Fig.14 shows the effect on the ion current density ratio and space potential along the presheath due to three electrical biases applied to the perturbing object:(1)$\sim$ 80 V positive bias; (2)$\sim$ 40 V negative bias with respective to the local floating potential; and (3) no bias(at a floating potential of $\sim -60V$ relative to the chamber wall). Negative bias of the object causes the space potential to be lowered uniformly in the presheath zone, retaining roughly the same spatial variation as in the no bias case. In contrast, positive bias not only raises the space potential everywhere in the presheath zone but also results in a change in sign of the presheath electric field. The electric field acts to draw electrons to the object and repel ions. Thus the usual picture of ions being accelerated to sound speed at the sheath edge of the object does not apply for the positive bias case. Nonetheless, similar ion current density ratios are observed.

One possible explanation for this result is that the cross-field transport into the magnetized probe's flux tube depends on the overall bias applied to the flux tube. The flux tube of the upstream-facing probe is intercepted by the probe itself and by the electrically insulated 'dump'. (Although the probe's collection length along the field line is much shorter than the distance to the dump.) On the other hand, the flux tube of the downstream-facing probe is intercepted by the probe itself and positively bias object. Experiments have shown that cross-field transport into a flux tube in PISCES plasma can be greatly reduced by applying a positive bias to the intercepting wall surface[26]. Thus the current ratio does not indicate a plasma flow velocity for the positive bias case but rather a decrease in the cross-field transport and, consequently, the net ion collection on the downstream-facing probe. It appears to be coincidental that a similar magnitude of ion current density ratios are obtained for positive as well as negative and no bias cases.

IV. CONCLUSIONS

Plasma flow velocity and density along the presheath have been deduced from the measured sheath current density and plasma potential by using the versatile fast-scanning probe.

The experimental data is best fit self-consistently with cross-field diffusivity about 4 times larger than Bohm. The fit suggests that shear viscosity plays an important role in interpreting the data along the presheath of the magnetized plasma, and it seems to be of order $\nu \sim 0.5nm_iD_\perp \sim 2.0nm_iD_{Bohm}$.

When changing the applied magnetic field, we observed that the cross-field diffusivity is does not scale like Bohm's formula, rather it is approximately proportional to $(D_{Bohm})^{1/2}$, the strongest dependence being magnetic field.

Little effect on the flow velocity is observed from a negative bias applied to the perturbing object. For a positively biased object, the presheath does not form. Even though the sheath current density ratio is observed to be similar to that of the no-bias or the negative-bias case, this does not indicate a flow velocity, but a decrease of ion collection on the downstream-facing probe.

It might be worthwhile to pursue further the following as future work:

A convincing calibration of the magnetized Mach probe requires an independent flow velocity measurement. Laser-induced fluorescence might offer an appropriate measurement.

There is a strong need to develop also a more reliable theory for the unmagnetized probe in a flowing plasma. If that were available, we could calibrate the present data of the magnetized Mach probe by the unmagnetized.

More reliable potential measurement technique should be developed to obtain the space potential accurately because it plays an important role in the presheath measurement. The use of a differential emissive probe may be appropriate.

Further study on positive bias effects are needed.

Acknowledgements

We would like to thank B. Lipschultz for many helpful discussions. We are very grateful to R. Lehmer and L. Schmidt for helping in the operation of the PISCES facility, to A. Pospieszczyk and Y. Ra for helping in measurement of the ion temperature, and to the PISCES technical staff, especially T. Sketchley, G. Gunner, and J. Elverum for assistance in hardware and electronics, and K. Andrews for computer and data acquisition systems support. We thank R. Childs in the Alcator group for his timely provision of the 6-hole alumina. One of us(KSC) greatly appreciates the opportunity to work with the PISCES group. This work was supported under the U.S. Department of Energy Contracts DE-AC02-78ET51013 and DE-FG03-86ER52134.

APPENDIX : Calibration of Probe Area

The PISCES facility is used for both materials and physics experiments. There are lots of impurities in the plasma such as carbon, copper, and tungsten. There are also strong interactions between the plasma and probe material. We, therefore, expect surface modification of probe during the measurement (normally one scan along the magnetic field takes about 2 to 3 hours). Even if we could measure the 'exact' probe area(in fact it is not possible to do this due to typical probe geometries), this does not guarantee the 'effective' collection area. Hence we need to calibrate the probe area for each scan by performing measurements with the probe head facing in opposite directions, normal and reversed.

For normal orientation at the middle of the scanning distance, define I_u^n and I_d^n as the measured ion current for the upstream and the downstream cases, respectively. And let I_u^r and I_d^r be those obtained when the entire probe is reversed.

We want to obtain actual current densities, by dividing by the effective probe areas:

$$J_u^n = \frac{I_u^n}{a_1},$$

$$J_d^n = \frac{I_d^n}{a_2},$$

$$J_u^r = \frac{I_u^r}{a_2},$$

$$J_d^r = \frac{I_d^n}{a_1},$$

where sub- and super-scripts n, r, u, and d mean 'normal orientation','reverse orientation','upstream', and 'downstream' , respectively. a_1 is the probe area which is away from the perturbing object in normal orientation, so it collects the ions on the upstream side. And a_2 is toward the object, so it collects the downstream ions.

Since the flow velocity should be same at the same position, whether the probes are reversed or not, the current density ratios should be the same, i.e.,

$$R = \frac{J_u^n}{J_d^n} = \frac{J_u^r}{J_d^r}.$$

Then

$$\frac{a_2}{a_1} = \left(\frac{I_u^r / I_d^r}{I_u^n / I_d^n}\right)^{1/2},$$

and

$$R = \left(\frac{I_u^n I_u^r}{I_d^n I_d^r}\right)^{1/2}.$$

For the absolute value of area a_1 we use the geometrical measurement. The average values of a_2/a_1 were found to be $\approx 1.2 \pm 0.3$ and 0.9 ± 0.1 for the magnetized probe and the unmagnetized probe, respectively.

REFERENCES

1) G.M.McCracken and P.E.Stott, Nucl. Fusion 19, 889(1978).

2) G.M.McCracken, International School of Plasma Physics Course on Diagnostics for Fusion Reactor Conditions, VolII(Varenna, 1982) p.419.

3) F.Wagner, *et al*, Phys. Rev. Lett. 49, 1408(1982).

4) G.M.McCracken, S.J.Fielding, and H.Ohtsuka, J. Nucl. Mater. 111&112, 396(1982)

5) J.Neuhauser, K.Lackner, and R.Wunderlich, Rep. IPP-1/198, Max-Planck-Institute fur Plasmaphysik, Garching(1982).

6) S.K.Erents, *et al*, Nucl. Fusion 26, 1591(1986).

7) S.K.Erents, *et al*, Nucl. Fusion 28, 1209(1988).

8) P.J.Harbour and G.Proudfoot, J. Nucl. Mater. 121, 222(1984).

9) P.C.Stangeby, in *Physics of Plasma – Wall Interactions in Controlled Fusion*, edited by D.E.Post and R.Behrisch(Plenum,1986) p.41.

10) A.S.Wan, B.LaBombard, B.Lipschultz, and T.F.Yang, J. Nucl. Mater. 145 – 147, 191(1987).

11) G.Proudfoot, P.J.Harbour, J.Allen and A.Lewis, J. Nucl. Mater. 128&129, 180(1984).

12) P.C.Stangeby, J. Phys. D: Applied Phys. 15, 1007(1982).

13) P.C.Stangeby, Phys. Fluids 27, 2699(1984).

14) G.F.Matthews, P.C.Stangeby, and P.Sewell, J. Nucl. Mater. 145 – 147, 220(1987).

15) B.LaBombard *et al*, Will be published in the Journal of Nuclear Materials.

16) D.M.Goebel, G.Campbell, and R.W.Conn, J. Nucl. Mater. 121, 277(1984)

17) I.H.Hutchinson, Phys. Fluids 30, 3777(1987).

18) I.H.Hutchinson, Phys. Rev. A 37, 4358(1988).

19) M.Laux *et al*, Proceedings of 8th International Conference on Plasma Surface Interactions in Controlled Fusion Devices, May, 1988, Julich, Federal Republic of Germany.

20) K-S.Chung and I.H.Hutchinson, Phys. Rev. A 38, 4721(1988).

21) K-S.Chung and I.H.Hutchinson, in preparation.

22) D.M.Goebel, Y.Hirooka, and T.A.Sketchly, Rev. Sci. Instrum. 56, 1717(1985).

23) R.Lehmer, private communication

24) F.F.Chen, *Electric Probes*, in *Plasma Diagnostic Techniques*, R.H.Huddlestone and S.L.Leonard eds. (Academic Press, N.Y., 1965) Chap. 4.

25) M.Hudis and L.M.Lidsky, J. Appl. Phys. 41, 5011(1970).

26) B.Labombard, R.Lehmer, K.S.Chung, R.W.Conn, Y.Hirooka, and R.E.Nygren , Bull. Amer. Phys. Soc. 33, 2103(1988).

Figure Captions

Fig. 1 Schematic setup for plasma flow experiment

Viewing port A is for controlling the position of Langmuir probe, and port B and C are used for arranging the perturbing object and fast-scanning probe. OMA stands for optical multichannel analyzer and GEA means gridded energy analyzer.

Fig. 2 Generation of presheath and main diagnostics

The presheath(shaded region) is generated by inserting a perturbing object, small compared to plasma size, into the middle of plasma column. The fast-scanning versatile probe is for the measurement of ion current, density, and potential. The OMA is used for ion temperature. Stationary Langmuir probe is for density and electron temperature.

Fig. 3 Fast-scanning versatile probe drive

The fast-scanning versatile probe drive is movable in the y and z directions. The Y-Z table is sealed by differential pumping. This system can access any point in a 10x10x10 cm volume.

Fig. 4 Versatile probe tip

The emissive and the unmagnetized Mach probes are made of 1% thoriated tungsten,

0.25 mm in diameter, and the magnetized Mach probe is molybdenum wire, 1 mm in diameter. Units are in mm.

Fig. 5 Sheath current density versus plasma column radius(x) and axial position along the magnetic field(z)

Current density(Amp/cm^2) measured by the magnetized probe(A) and the unmagnetized probe(B) at the downstream side. The perturbing object is located at x=0 cm. The magnetic field is applied along the z direction. Conditions are : $B = 1400G$, $T_e = 10eV$, $T_i = 0.8eV$, $n_\infty = 2 \times 10^{12} cm^{-3}$, neutral He pressure $\sim 1 \times 10^{-3}$ torr.

Fig. 6 Potential versus plasma column radius(x) and axial position along the magnetic field(z)

(A) shows the "space" potential measured by the emissive probe during hot emission, and (B) indicates the floating potential taken while it is not emitting. Conditions are : $B = 1400G$, $T_e = 10eV$, $T_i = 0.8eV$, $n_\infty = 2 \times 10^{12} cm^{-3}$, neutral He pressure $\sim 1 \times 10^{-3}$ torr.

Fig. 7 Current densities, current density ratios, and potentials along z at the center of the object

(A) Upstream(MU) and downstream(MD) sheath current densities(Amp/cm^2) mea-

sured by the magnetized Mach probe. Two data points at the same position indicate measurements while the emissive probe is emitting and non-emitting: (B) Those for the unmagnetized Mach probe: (C) Sheath current density ratios for the magnetized(M) and the unmagnetized(U) Mach probes: (D) "Space"(S) and floating(F) potentials(Volt). Conditions are : $B = 1400G$, $T_e = 10eV$, $T_i \simeq 0.8eV$, $n_\infty = 2 \times 10^{12} cm^{-3}$, neutral He pressure $\sim 1 \times 10^{-3}$ torr.

Fig. 8 Interpretation of measured data

Two presheaths are formed, one is due to the perturbing object, the other is due to versatile probe tip. The unperturbed parameters along the presheath due to object are to be deduced from the measured sheath current densities of each direction(upstream and downstream).

Fig. 9 Flow velocity along the presheath

Deduced flow velocity according to various models. Flow velocity is normalized by $[(T_e + T_i)/m_i]^{1/2}$. ▲ Stangeby's fluid model[13] equivalent to $\alpha = 0.0$ in kinetic model, ■ Hutchinson's fluid model[17] equivalent to $\alpha = 1.0$, ● kinetic[21] model with $\alpha = 0.5$ for the magnetized probe, ○ Hudis and Lidsky's fluid model[25] for the unmagnetized probe, and □ free-fall model[15]. Conditions are the same as in Fig. 5.

and 16 mm, $B = 1000 - 1400G$, $T_e = 7 - 10eV$, $T_i \simeq 0.8eV$, $n_\infty = 2 - 4 \times 10^{12} cm^{-3}$.

Solid line is from a kinetic model with $\alpha = 1.0$ and dotted line is with $\alpha = 0.0$.

Fig. 13 Magnetic field effect

(A) Sheath current density ratios are measured along the presheath by the unmagnetized Mach probe(in real distance).

(B) Sheath current density ratios are measured along the presheath by the unmagnetized Mach probe(in normalized distance). Conditions are following: $T_e = 6 - 9eV$, $n_\infty = 3 - 4 \times 10^{12} cm^{-3}$, B = 400(□), 600(●) , 800(△), 1000(■), 1200(○), 1400(▲) G.

Fig. 14 Electrical bias effect

(A) Sheath current density ratios. (B) "Space" potentials. (C) Normalized "space" potentials by $-T_e/e$ relative to last point as zero. Here ■ $\sim -80V$, ○ $\sim +40V$ relative to floating potential is applied to the perturbing object. ▲ is floating case.

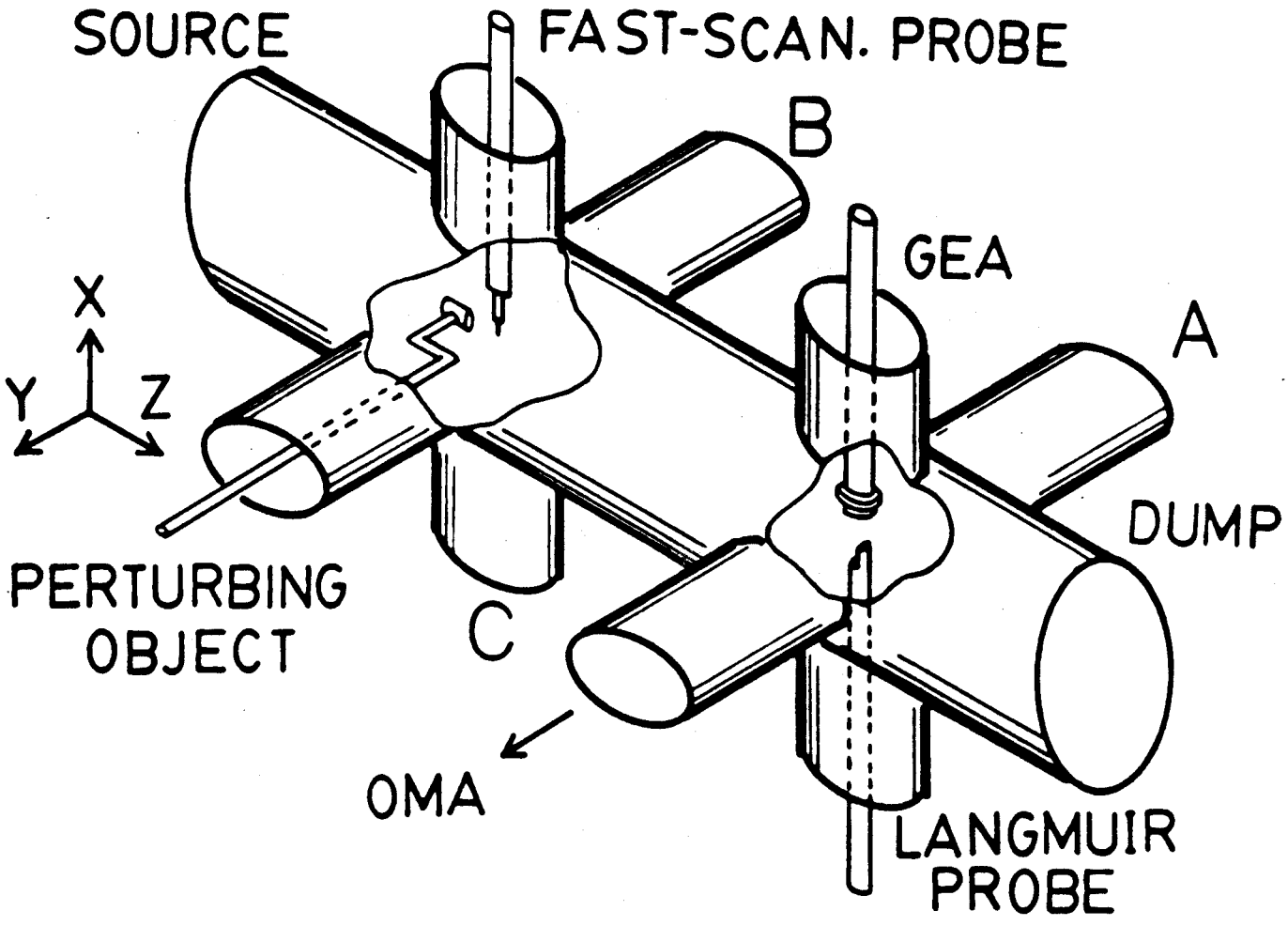

Fig. 1 Schematic setup for plasma flow experiment

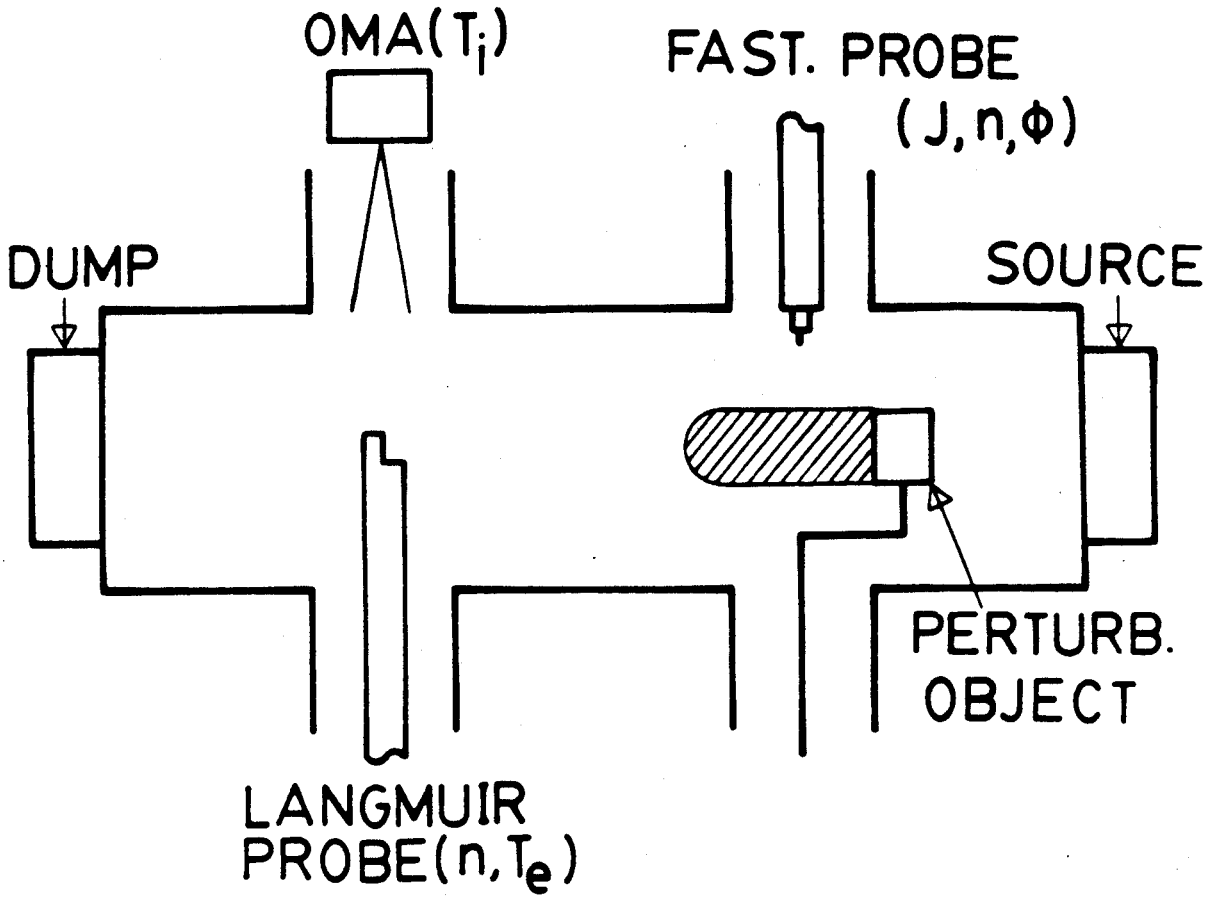

Fig. 2 Generation of presheath and main diagnostics

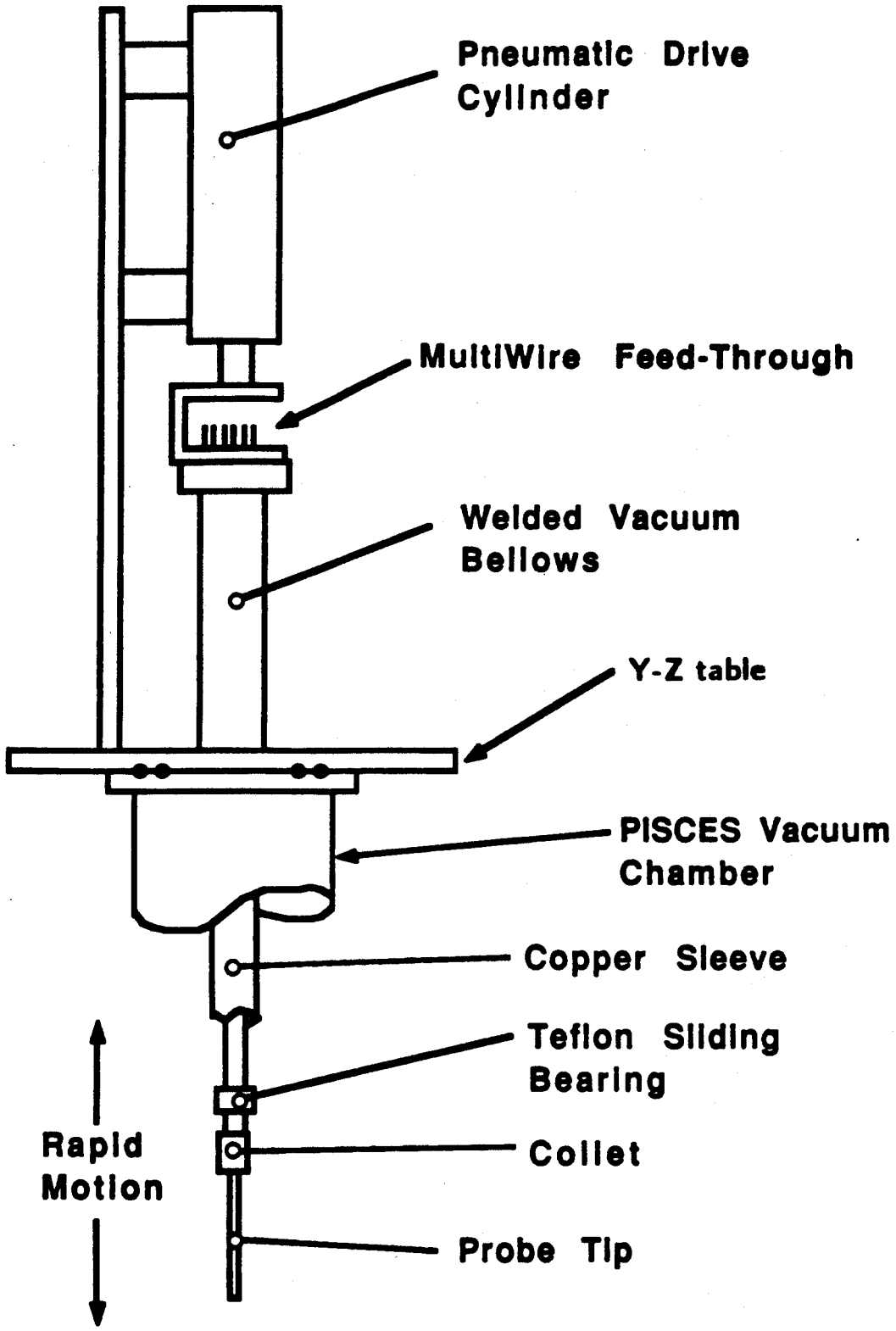

Fig. 3 Fast-scanning versatile probe drive

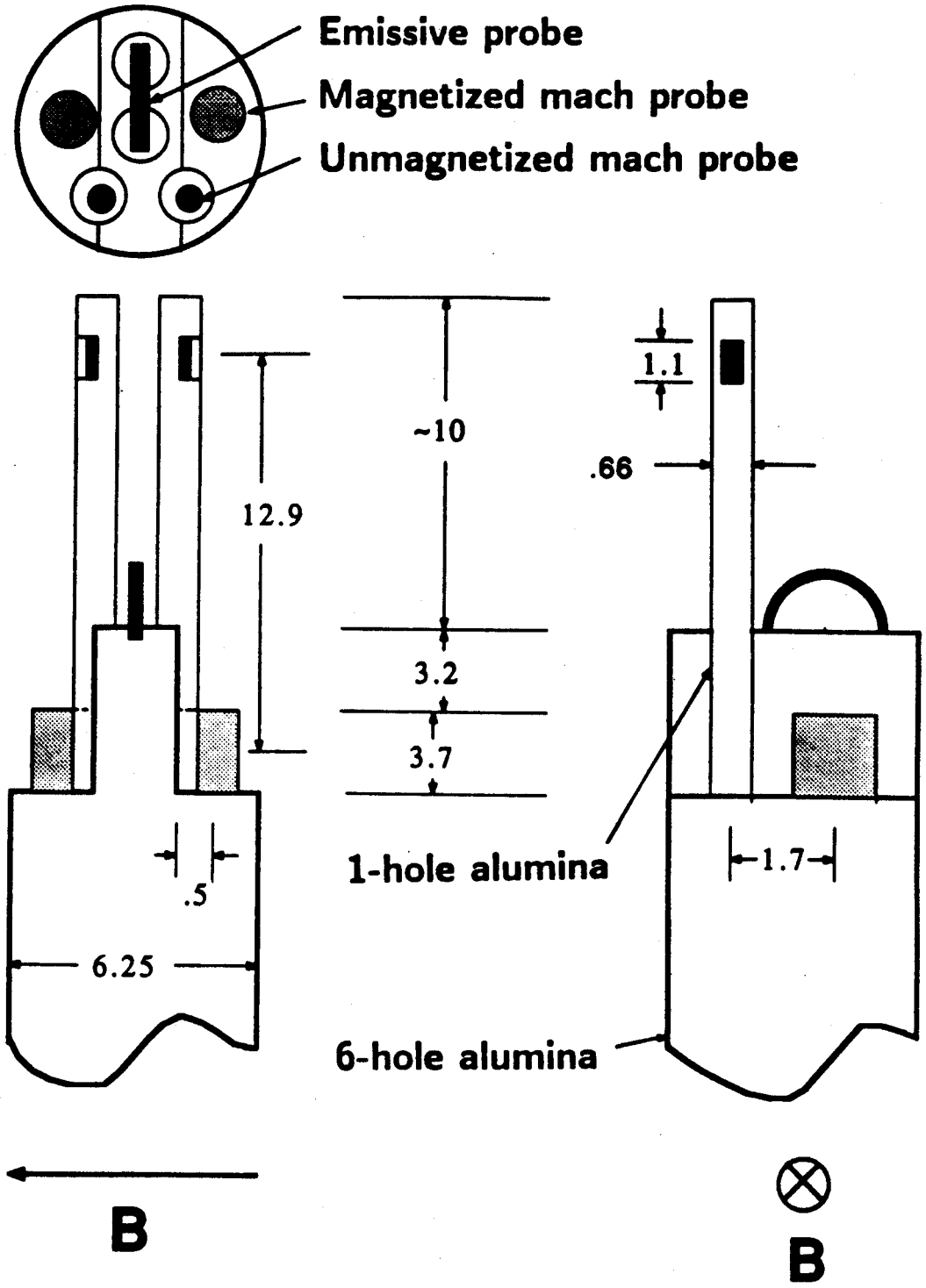

Fig. 4 Versatile probe tip

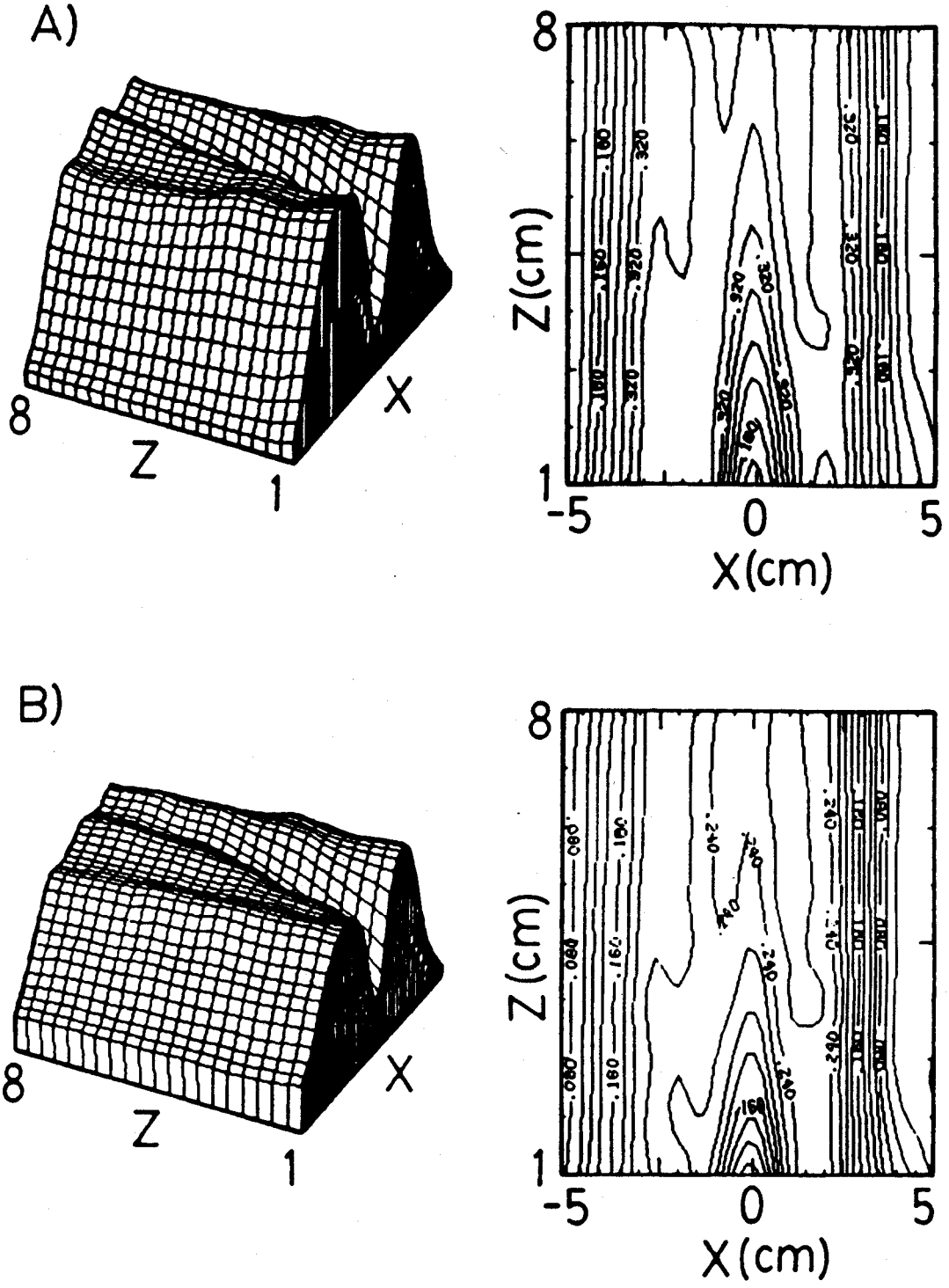

Fig. 5 Sheath current density versus plasma column radius(x) and axial position along the magnetic field(z)

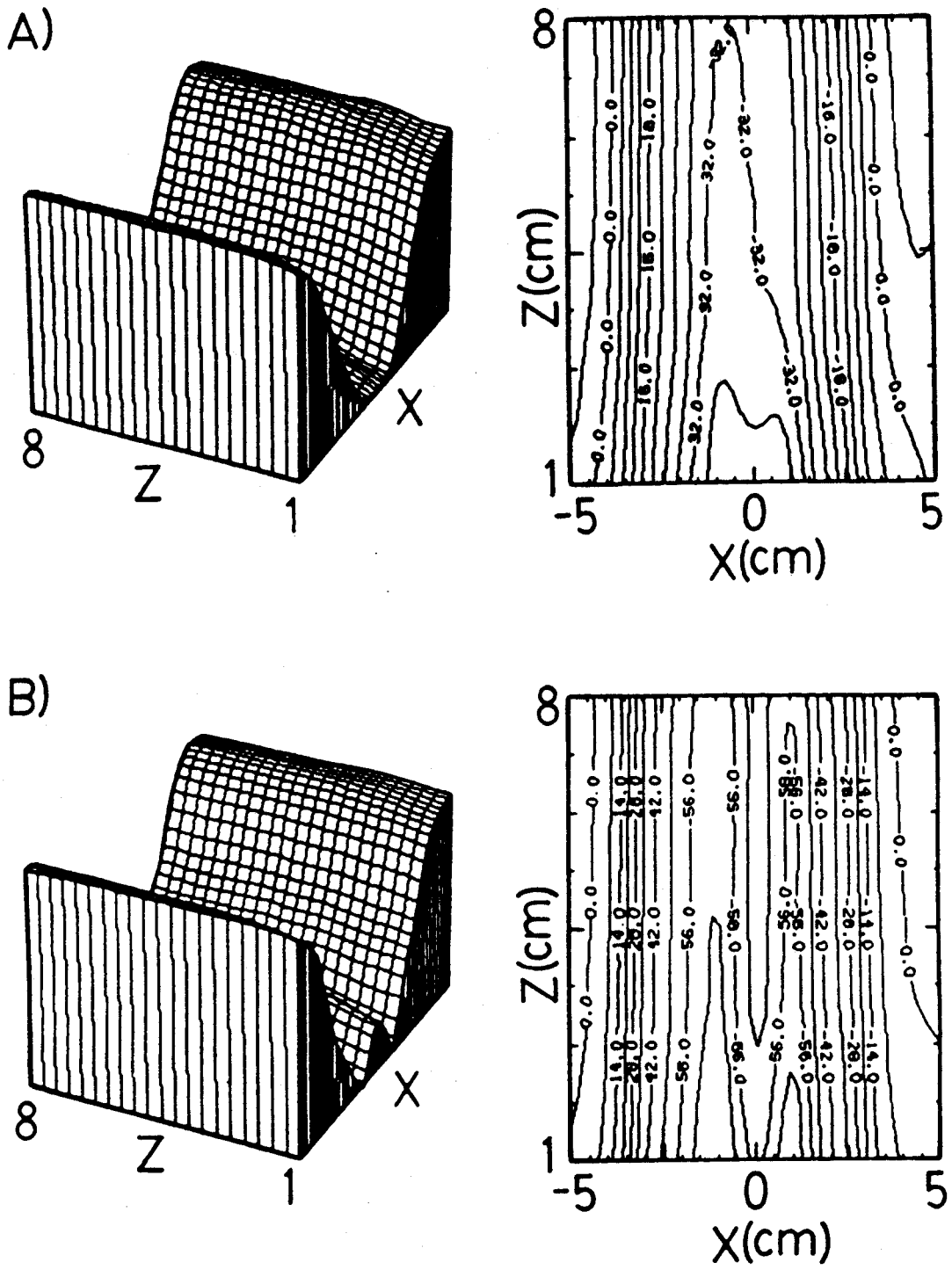

Fig. 6 Potential versus plasma column radius(x) and axial position along the magnetic field(z)

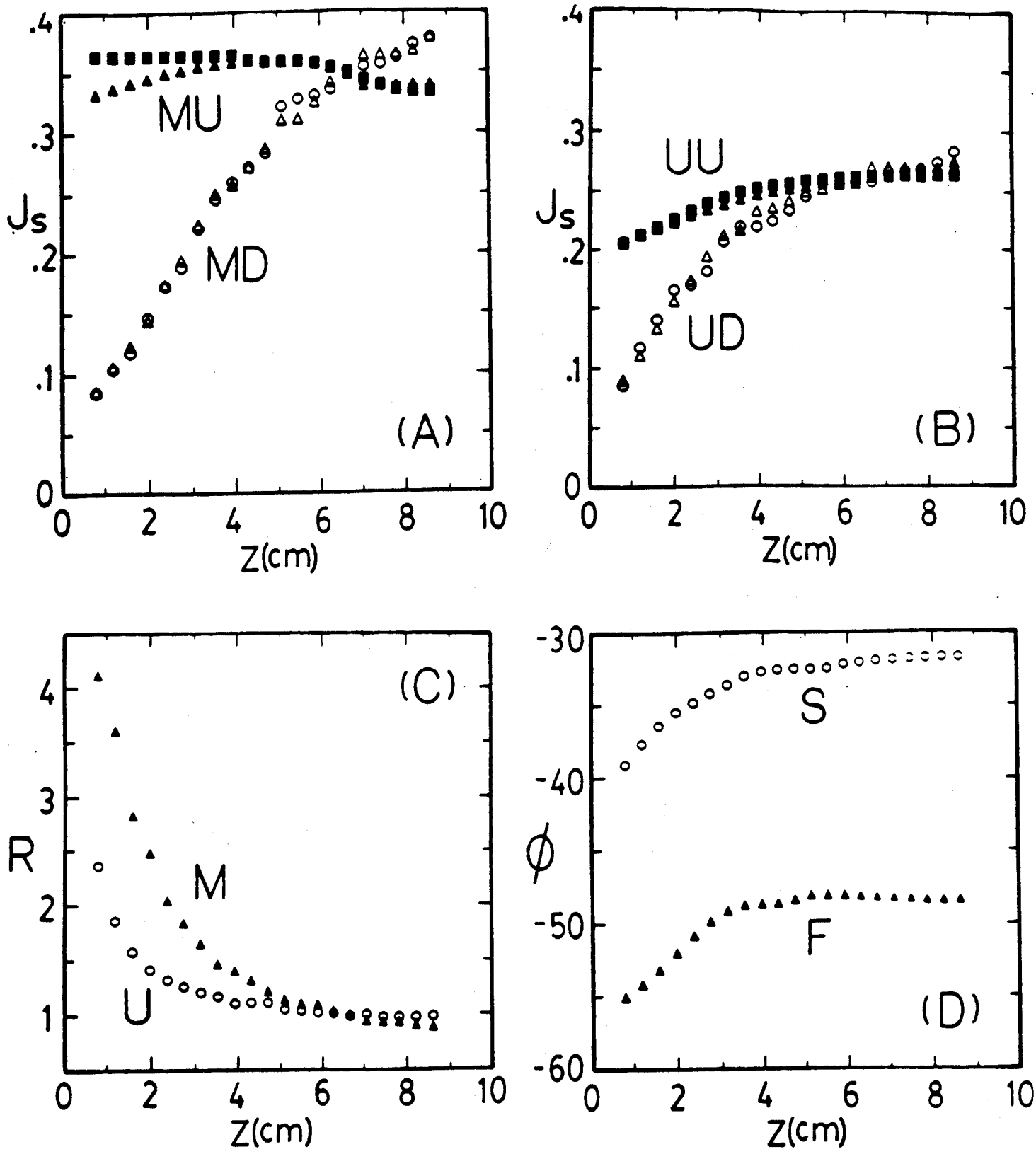

Fig. 7 Current densities, current density ratios, and potentials along z at the center of the object

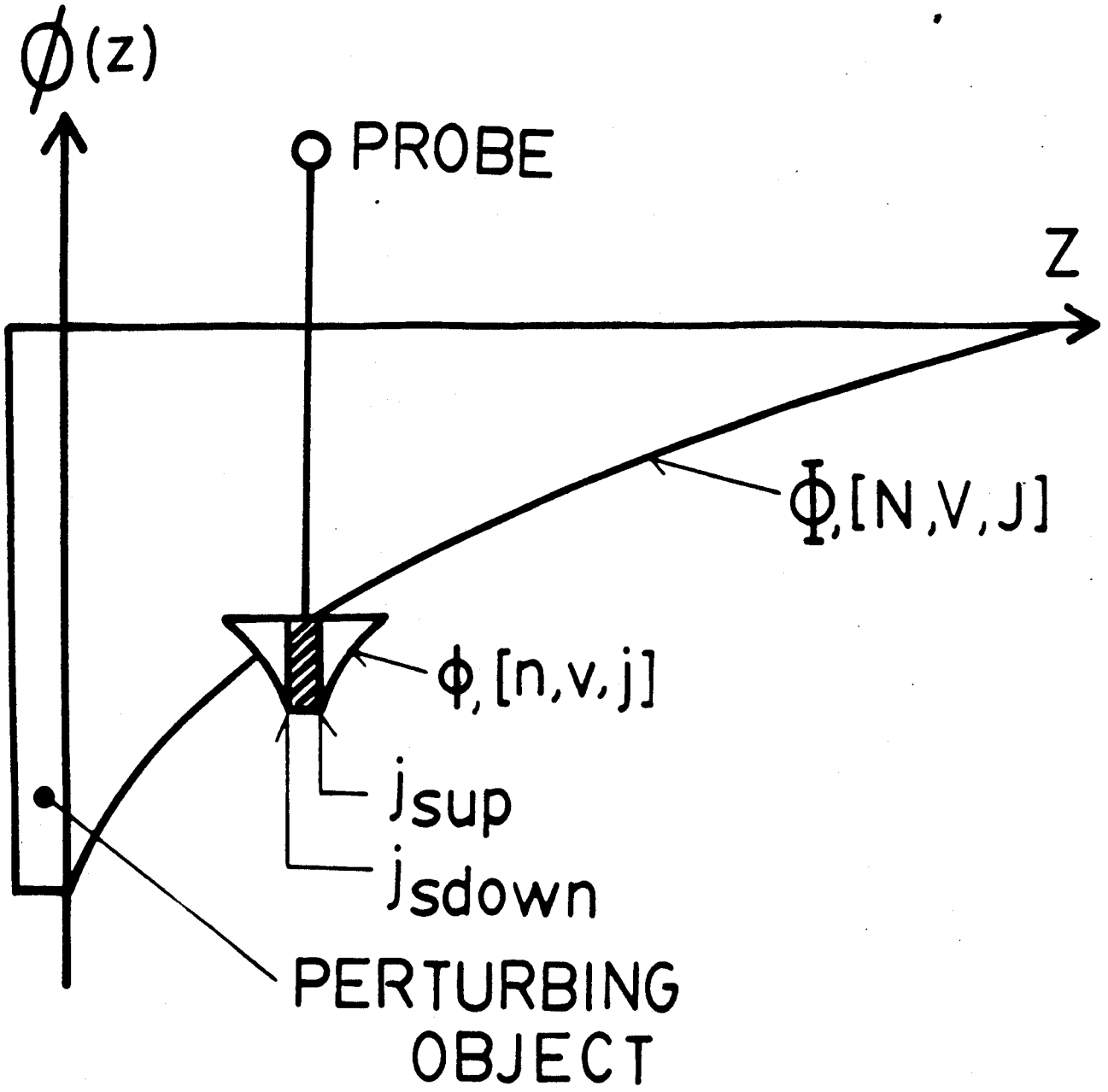

Fig. 8 Interpretation of measured data

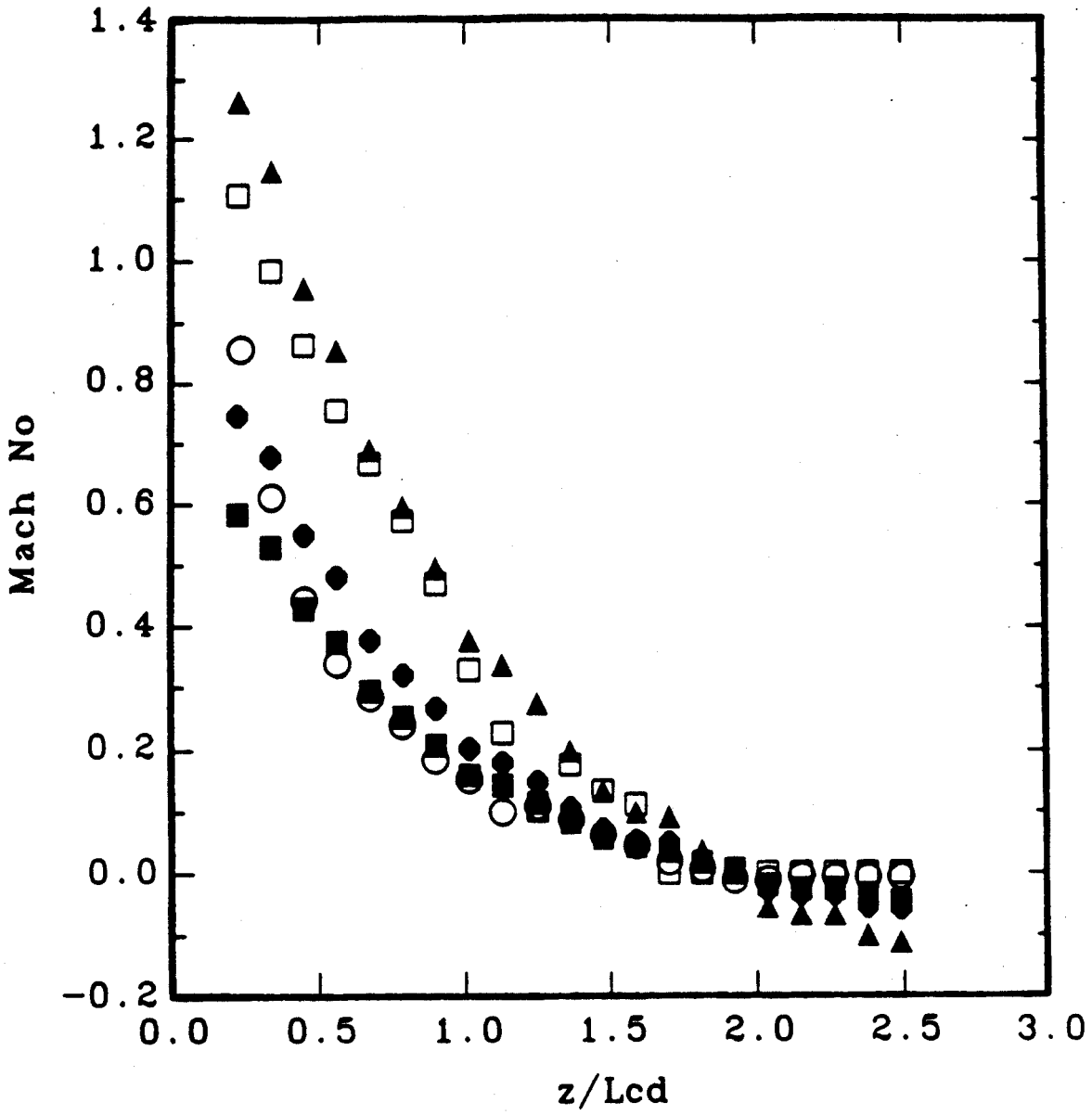

Fig. 9 Flow velocity along the presheath

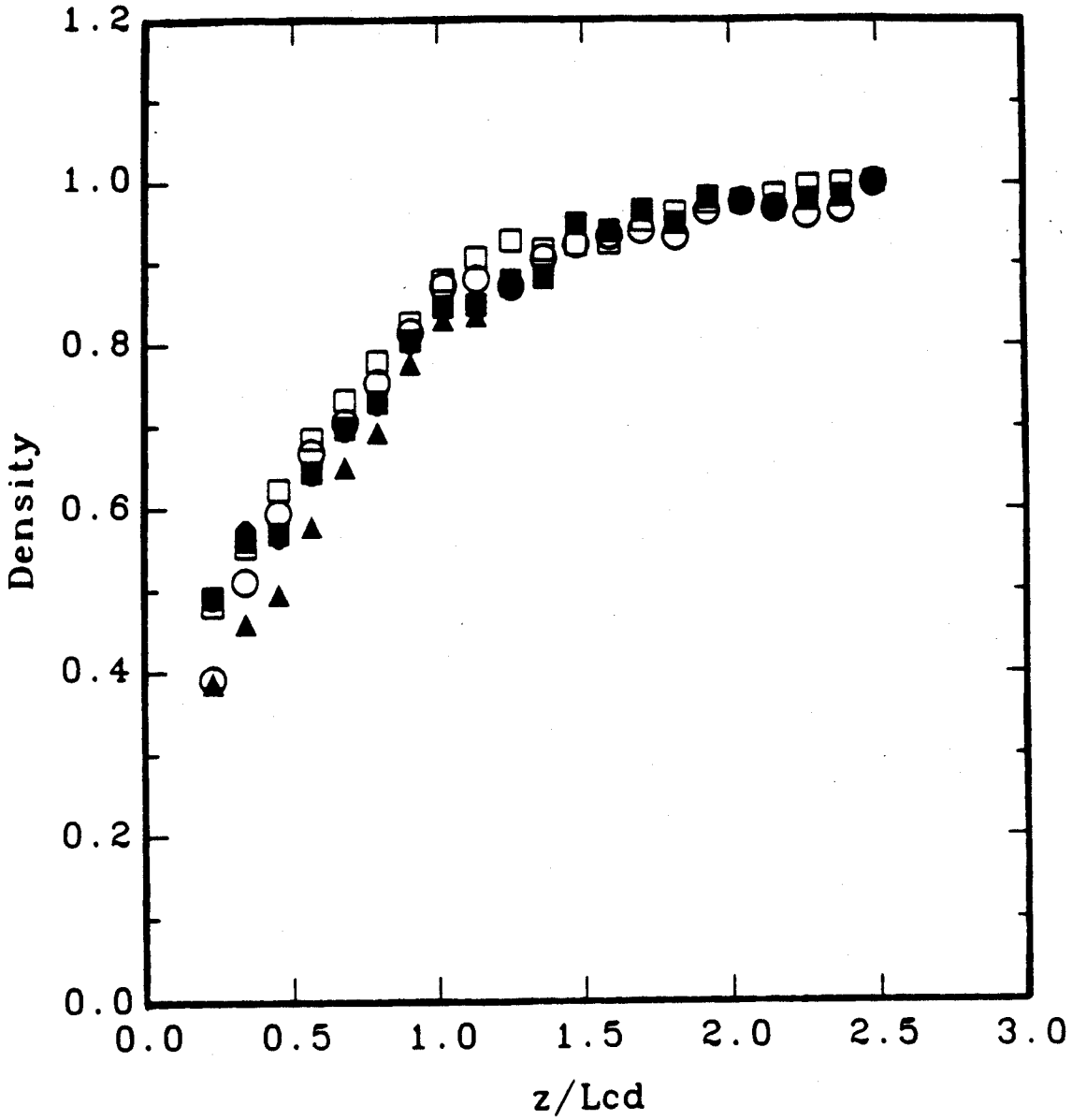

Fig. 10 Density along the presheath

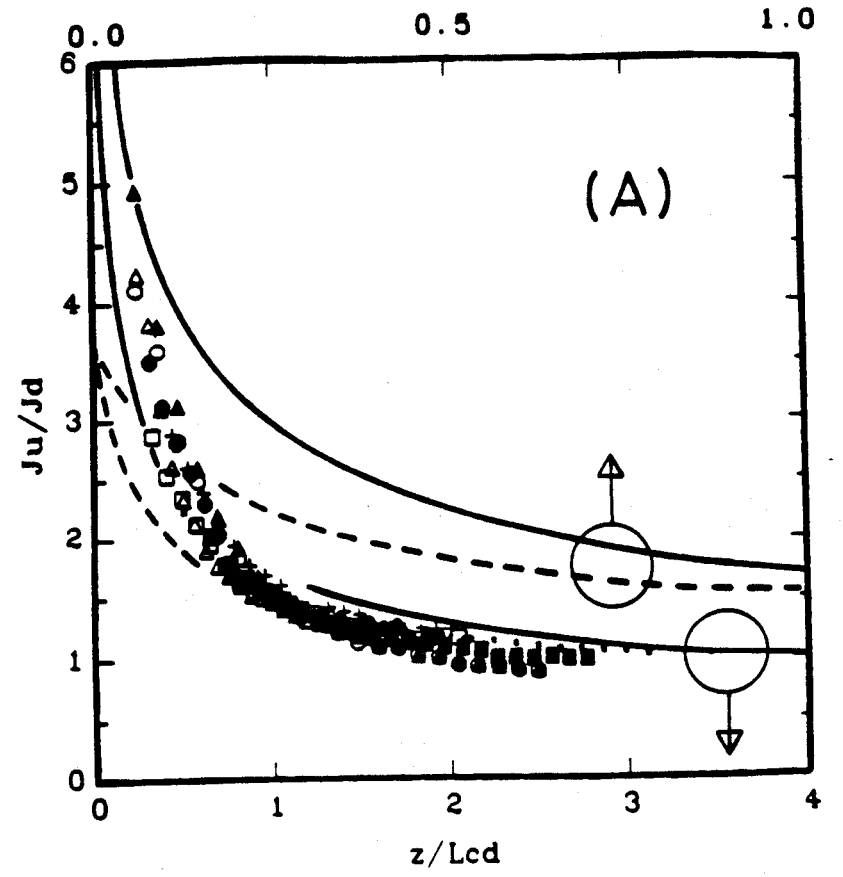

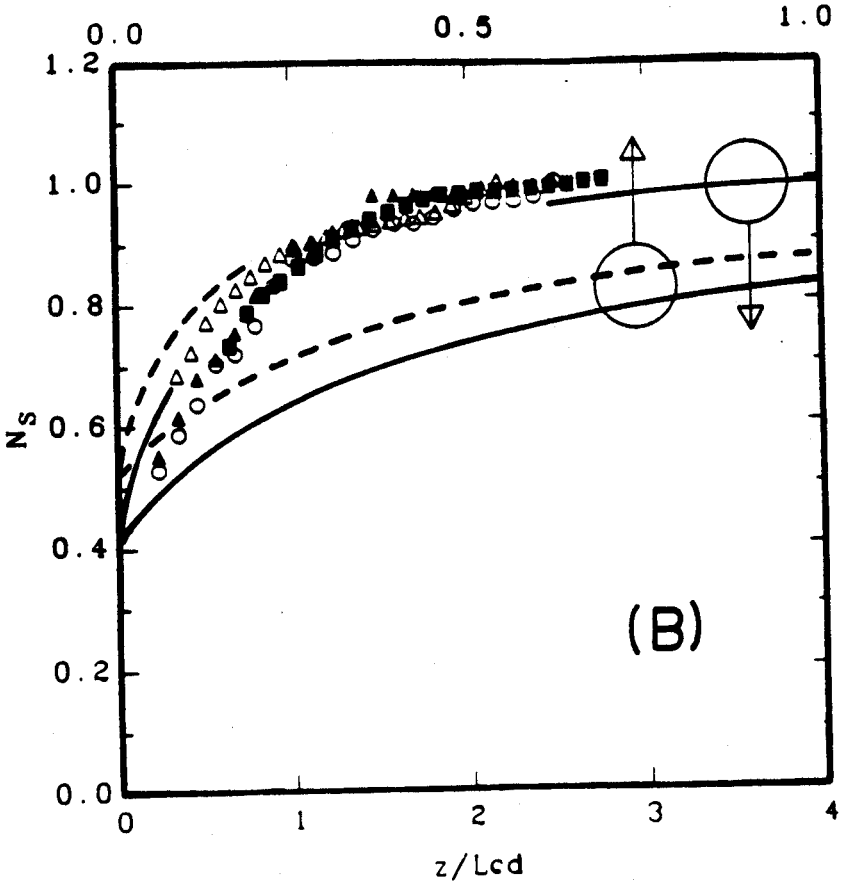

Fig. 11 Measured current ratios and densities ($D_\perp = D_{Bohm}, 4D_{Bohm}$)

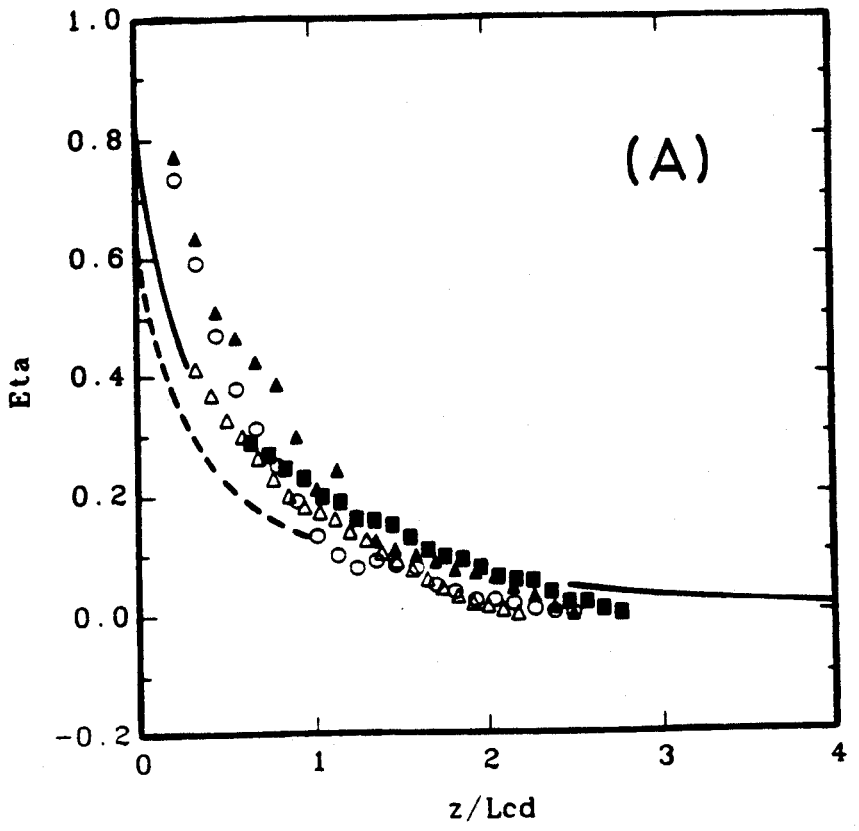

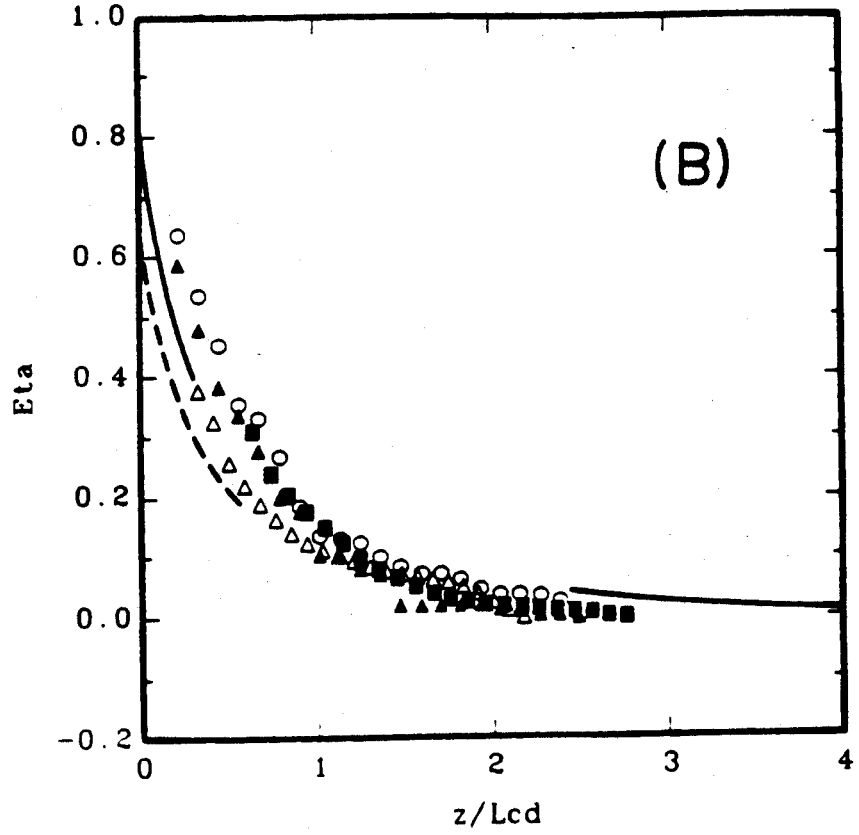

Fig. 12 Potentials along the presheath($D_\perp = 4D_{Bohm}$)

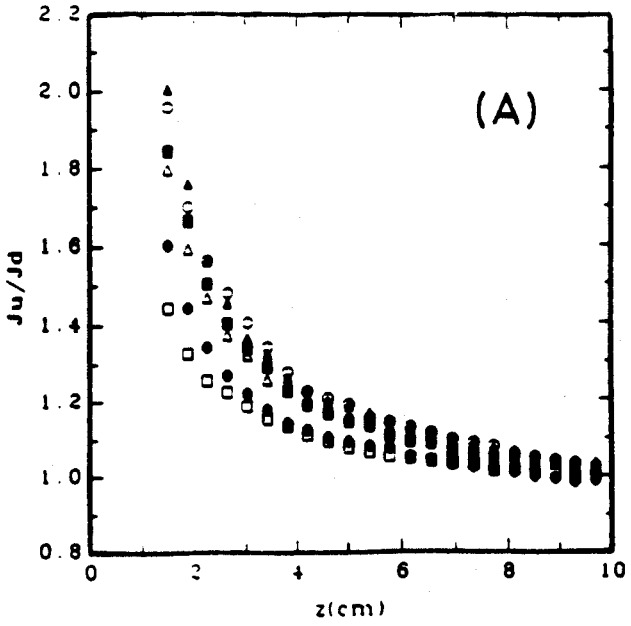
(A)
Ju/Jd
z(cm)

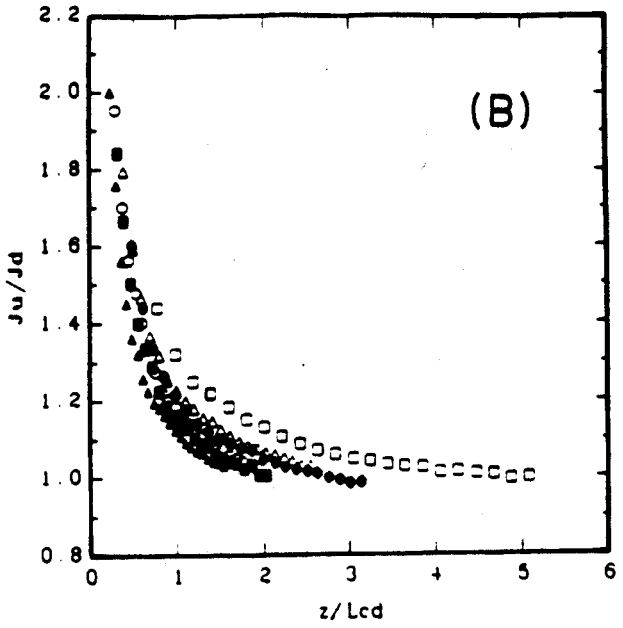
(B)
Ju/Jd
z/Lcd

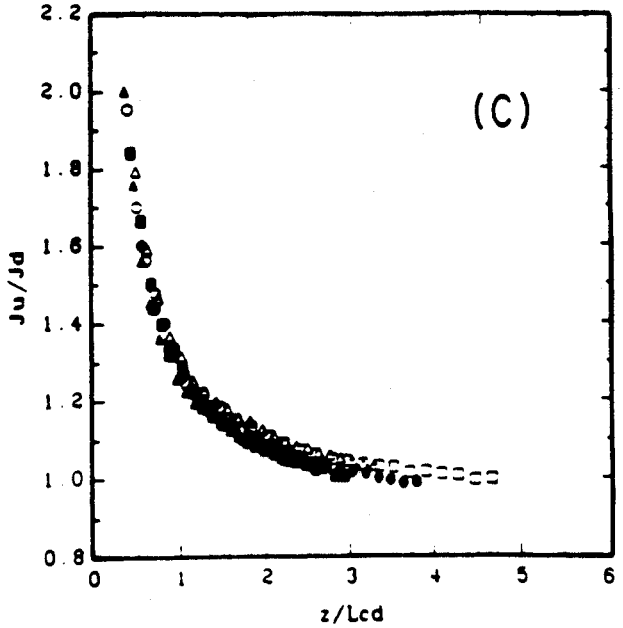
(C)
Ju/Jd
z/Lcd

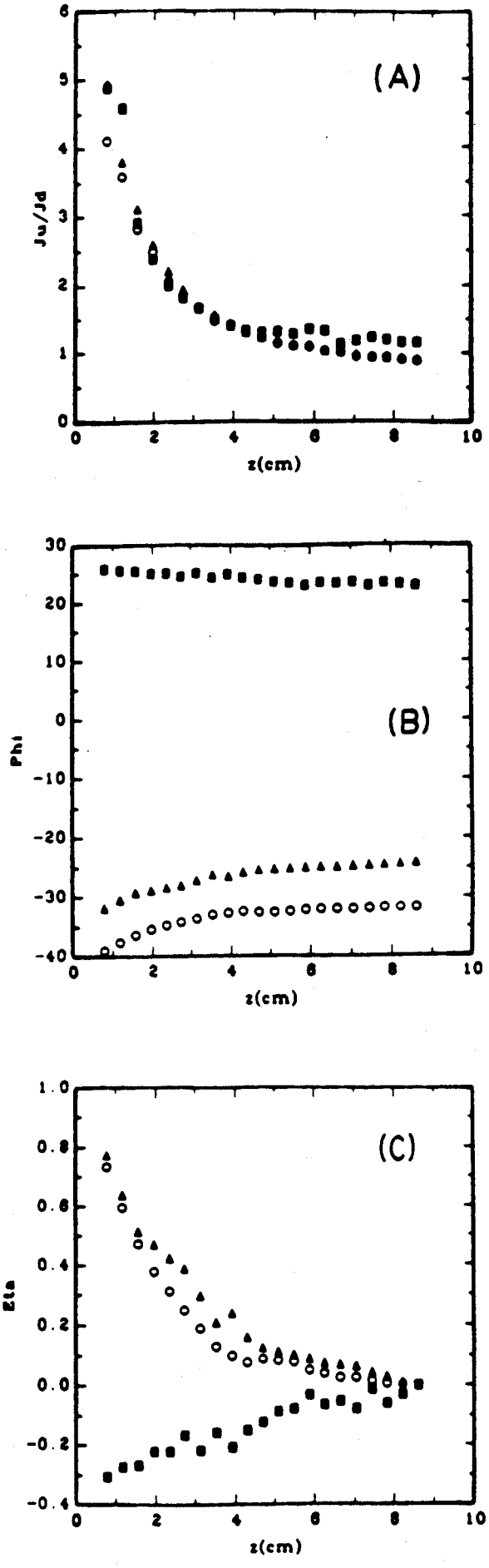

Fig. 14 Electrical bias effect